universe

IMPACT FACTOR 2.9

CITESCORE 3.6

Communication

Pion Interferometry with Lévy-Stable Sources in $\sqrt{s_{NN}}$ = 200 GeV Au + Au Collisions at STAR

Dániel Kincses

Special Issue
Multiparticle Dynamics

Edited by
Prof. Dr. Tamás Csörgő, Prof. Dr. Máté Csanád and Dr. Tamás Novák

MDPI

https://doi.org/10.3390/universe10030102

universe

MDPI

Communication

Pion Interferometry with Lévy-Stable Sources in $\sqrt{s_{NN}}$ = 200 GeV Au + Au Collisions at STAR

Dániel Kincses on behalf of the STAR Collaboration

Institute of Physics, ELTE Eötvös Loránd University, Pázmány Péter Sétány 1/A, H-1117 Budapest, Hungary; kincses@ttk.elte.hu

Abstract: Measurements of femtoscopic correlations in high-energy heavy-ion collisions are used to unravel the space–time structure of the particle-emitting source (the quark–gluon plasma). Recent results indicate that the pion pair source exhibits a power law behavior and can be described well by a Lévy distribution. In this study, Lévy fits were applied to the measured one-dimensional two-pion correlation functions in Au + Au collisions at $\sqrt{s_{NN}}$ = 200 GeV. The three extracted source parameters are the Lévy scale parameter, R, which relates to the size of the source; the correlation strength parameter, λ; and the Lévy exponent, α, which characterizes the power law tail of the source. In this paper, we report the current status of the analysis of the extracted Lévy source parameters and present their dependence on average transverse mass, m_T, and on centrality.

Keywords: femtoscopy; heavy-ion physics; Lévy distribution; quantum–statistical correlations

Citation: Kincses, D., on behalf of the STAR Collaboration. Pion Interferometry with Lévy-Stable Sources in $\sqrt{s_{NN}}$ = 200 GeV Au + Au Collisions at STAR. *Universe* **2024**, *10*, 102. https://doi.org/10.3390/universe10030102

Academic Editor: Giuseppe Verde

Received: 23 January 2024
Revised: 8 February 2024
Accepted: 15 February 2024
Published: 20 February 2024

1. Introduction to Femtoscopic Correlations

One of the indispensable tools aiding in the quest to explore the matter created in high-energy collisions of heavy nuclei is femtoscopy [1–6]. Femtoscopy utilizes quantum statistics and final-state interactions to make a connection between momentum correlations and spatial correlations. Its name was coined because, with the help of such correlation measurements, one can map the space–time geometry of the particle-emitting source on the femtometer scale. In the following, we review some of the basic definitions of femtoscopic correlation functions and discuss the shape of the two-particle source. Although femtoscopic techniques can be applied to a large variety of particle combinations [7,8], in this paper, we focus on two-particle correlations of identical pions, and thus, we introduce the following definitions accordingly.

Utilizing the $q = p_1 - p_2$ relative pair momentum and the $K = 0.5(p_1 + p_2)$ average pair momentum variables, the two-particle momentum correlation function $C_2(q, K)$ can be expressed with the pair source function $D(r, K)$ and the symmetrized pair wave function $\psi_q(r)$ as

$$C_2(q, K) = \int d^4r D(r, K)|\psi_q(r)|^2. \quad (1)$$

The pair wave function contains effects from quantum statistics and final-state interactions and can be calculated from the well-known quantum-mechanical Coulomb problem [9]. The pair source function $D(r, K)$ is defined with the $S(x, K)$ single-particle source function or phase space density (where r is the relative coordinate of the pair, and the smoothness approximation $p_1 \approx p_2 \approx K$ is utilized [10]) as follows:

$$D(r, K) = \int d^4\rho \, S\left(\rho + \frac{1}{2}r, K\right) S\left(\rho - \frac{1}{2}r, K\right). \quad (2)$$

The pair source $D(r, K)$ cannot be measured directly in experiments. However, utilizing Equation (1), measurements of the momentum correlation function can provide

information about the shape of the pair source. The latter, especially for pions, has been under the femtoscope for a long time. A commonly used assumption for the shape of the pion pair source was the Gaussian, or normal, distribution. However, there have been indications of a power law behavior [11,12], and recent studies both in phenomenology [13–16] and through experimentation [17–19] showed that the more general Lévy-stable distribution might provide a better description. In this paper, we present the latest preliminary results of Lévy source parameter measurements for the STAR experiment.

2. Lévy-Stable Source Distributions

As mentioned previously, observations of a significant tail in the pion source required a more general approach and a need to go beyond the Gaussian description. Lévy-stable distributions [20,21] (arising from the Generalized Central Limit Theorem [22]) in case of spherical symmetry are defined as

$$\mathcal{L}(\alpha, R; \boldsymbol{r}) = \frac{1}{(2\pi)^3} \int d^3\boldsymbol{q} e^{i\boldsymbol{q}\boldsymbol{r}} e^{-\frac{1}{2}|qR|^\alpha}, \tag{3}$$

where α is the Lévy exponent parameter, describing the tail of the distribution, and R is the Lévy scale parameter. Important properties of these stable distributions are the power law behavior for $\alpha < 2$, and the retaining of the same α value under convolution, i.e., if the single particle source is a Lévy distribution, the pair source will be one as well, with the same exponent.

Such distributions were found to be good candidates to describe experimental measurements [17–19], as well as the source shape in event generator models such as EPOS [13,14]. The reason for the appearance of the apparent $\alpha < 2$ power law behavior is yet to be understood in detail; at different collision energies and different collision systems, there can be many various competing phenomena, such as jet fragmentation [23,24], critical behavior [25], event averaging [26,27], resonance decays [13,14,28], and anomalous diffusion [28,29].

In the case of the top RHIC energy investigated in the current paper, anomalous diffusion (in terms of hadronic rescattering) and resonance decays are the most probable. Using EPOS simulations including UrQMD, it was shown that the latter cannot be the sole reason for the Lévy shape [13,14]; primordial pions after UrQMD also exhibit a power law behavior. It is also important to note that these analyses were performed on an event-by-event basis, and the Lévy shape appeared in individual events. Thus, (at least in EPOS) it is not the event averaging that is behind the appearance of the Lévy shape.

Another usual argument in the case of one-dimensional analyses is that angle-averaging leads to a non-Gaussian behavior. This is, of course, true; however, an angle-averaged non-spherical Gaussian is strikingly different from a Lévy distribution, as was demonstrated in the talks given by M. Csanád at the 52nd International Symposium on Multiparticle Dynamics and at the XVI Workshop of Particle Correlations and Femtoscopy. The details of those talks are also summarized in the same Special Issue as this paper [30]. In ref. [31], it was also shown that an angle-averaged experimental Lévy analysis led to the same α exponent as a three-dimensional measurement. The angle averaging for Lévy sources was also investigated in ref. [16].

In the absence of any final-state interaction, the correlation function is in direct connection with the Fourier transform of the pair source function [15]. Thus, for spherically symmetric Lévy sources, the correlation function takes the following form:

$$C_2(Q) = 1 + \lambda e^{-|RQ|^\alpha}, \tag{4}$$

where Q is the magnitude of the relative momentum variable. In Equation (4), the λ correlation strength parameter was also introduced to account for a possible change from unity (caused by, e.g., decays of long-lived resonances [32], partial coherence [4], or quasi-random electromagnetic fields [33]). The average momentum K dependence in Equation (4) appears

through the source parameters $\lambda(K)$, $R(K)$, and $\alpha(K)$. In experimental measurements, usually, instead of K, the average transverse mass is used, defined as $m_T = \sqrt{k_T^2 + m^2}$, where m is the particle mass and k_T is the transverse component of K.

In the case of identical charged pions (which are the subject of the current paper), one cannot neglect the Coulomb final-state interaction. Calculating the shape of the correlation function for Lévy-stable sources with the Coulomb-interacting pair wave function is not a trivial task; however, numerical calculations are possible, as detailed in ref. [15]. Taking into account the Coulomb interaction, Equation (4) can be modified to the following:

$$C_2(Q) = \left(1 - \lambda + \lambda \cdot K(Q; \alpha, R) \cdot \left(1 + e^{-|RQ|^\alpha}\right)\right) \cdot N(1 + \varepsilon Q), \tag{5}$$

where $K(Q; \alpha, R)$ is the so-called Coulomb correction factor (calculated numerically), and the $N(1 + \varepsilon Q)$ factor represents a possible linear background (usually negligible).

3. Data Analysis

In this section, we detail the process of the data analysis for STAR, in particular, the measurement and fitting of the two-particle correlation functions. The data set used for the analysis was recorded in 2011 by the STAR experiment in Au + Au collisions at $\sqrt{s_{NN}} = 200$ GeV center-of-mass collision energy. The minimum bias data contained about 550 million events.

The main detector of the STAR experiment is a time projection chamber (TPC) used for centrality determination, vertex position measurement, tracking, and particle identification, with specific ionization energy loss (dE/dx) [34]. Another important detector used in this analysis is the barrel Time Of Flight (bTOF) detector [35–37], which is used together with the TPC to reject pile-up events from the sample and also to aid in particle identification, especially at higher transverse momentum ranges.

After the event selection based on the criteria of vertex position and pile-up rejection, the next step was to select the charged pion tracks. The track selection criteria included the number of hits used to reconstruct the track in the TPC ($N_{\text{hits}} > 20$), the distance of closest approach to the primary vertex (DCA < 2.0 cm), pseudo-rapidity ($|\eta| < 0.75$), and transverse momentum ($0.15 < p_T[\text{GeV}/c] < 1.0$). For the pion identification, a combined approach was utilized using the dE/dx measured by TPC and the time-of-flight measured by TOF simultaneously. We found that this eliminates the need for veto cuts; however, when only TPC information was available, veto cuts for electrons, kaons, and protons were also utilized. In measurements where quantities such as relative and average momentum are calculated for pairs of particles, another important aspect is taken into account: the merging and splitting effects stemming from the track reconstruction algorithm [38]. For the latter, a cut on the splitting level quantity was used (SL < 0.6), similarly to ref. [38]. To correct for the merging effect, a cut on the fraction of merged hit (FMH) quantity was used (similarly to ref. [38]), requiring it to be less than 5 percent. Furthermore, the average separation of the pair was calculated over the TPC pad rows and was required to be greater than 3 cm.

To construct the correlation functions, the event mixing method was utilized, as described in, e.g., ref. [17]. When mixing pairs from separate events, both events were required to belong to the same event class, using 2 cm z-vertex bins and 5% centrality bins. Correlation functions were constructed for four centrality bins (0–10%, 10–20%, 20–30%, 30–40%), and for 21 average transverse momentum k_T bins, ranging from 0.175 GeV/c up to 0.750 GeV/c. The one-dimensional relative-momentum variable of choice was the magnitude of the three-momentum difference in the longitudinal co-moving system (LCMS) [16].

The systematic uncertainty investigations included variations of the previously detailed single-track and pair cuts and variations of the lower and upper fit limits. The effect of the choice of bin width in the relative momentum variable and the difference between $\pi^+\pi^+$ and $\pi^-\pi^-$ correlation functions were found to be negligible. Fitting of the

correlation functions was conducted using Equation (5) in an iterative, self-consistent way, similarly to what is described in ref. [17]. An example fit is shown in Figure 1. Similarly to Figure 1, all other fits also converged with a confidence level greater than 0.1%.

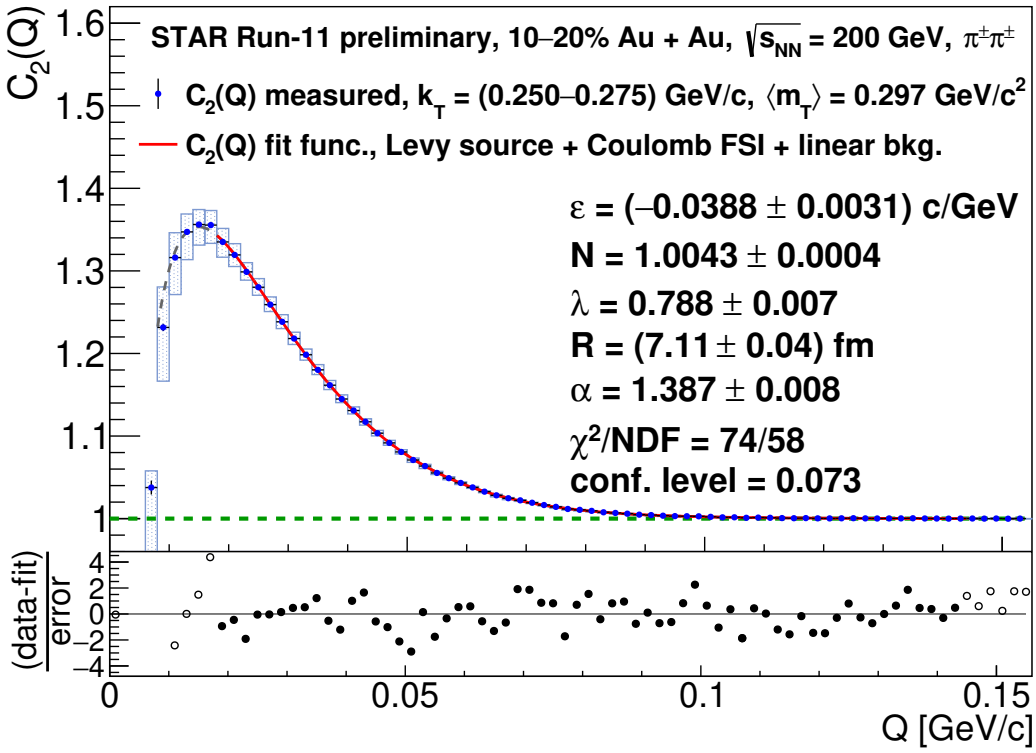

Figure 1. An example two-pion correlation function measured in $\sqrt{s_{NN}}$ = 200 GeV Au + Au collisions. The correlation function belongs to the 10–20% centrality class, with pion pairs having an average transverse momentum in the range of 0.250 GeV/c–0.275 GeV/c. The measured correlation function is denoted by dark blue data points with statistical uncertainties marked by error bars. The opaque blue boxes on the data points correspond to the systematic uncertainties stemming from single-track and pair cuts and variations. The fit function (corresponding to Equation (5)) is shown with a red curve within the fit range and with a gray dashed curve outside.

4. Results

In this section, we review the centrality and the average transverse mass (m_T) dependence of the extracted source parameters.

The Lévy exponent α as a function of m_T and centrality is shown in Figure 2. There is very little dependence on the average transverse mass; a constant fit provides a good description of $\alpha(m_T)$ for all four centrality classes. The values are far from the Gaussian ($\alpha = 2$) case and decrease with increasing N_{part} values, as shown in Figure 3. It is interesting to note that the CMS experiment observed an opposite trend with centrality [18], albeit with different kinematic selections and no particle identification; hence, a direct comparison is difficult. As α is highly anti-correlated with the other two fit parameters, this could be mirrored in the N_{part} dependence as well; as N_{part} (and the multiplicity) increases, the size of the system (and with that the R Lévy scale parameter) increases, while α decreases.

The Lévy scale parameter R is shown in Figure 4 with the four centrality classes on separate panels. The decreasing trend with m_T is very similar to the usual observations for Gaussian HBT radii [39] and might be attributed to the hydrodynamic expansion of the system [40–42]. Hydrodynamic calculations for Gaussian radii predict an $R \propto 1/\sqrt{m_T}$-type scaling. The PHENIX experiment found that this scaling holds for the Lévy-scale parameter as well [17]; however, with the level of precision available for the STAR experiment, this may no longer hold. Figure 4 includes fits to the transverse mass dependence parameterized

as $R(m_T) = R_0(Am_T + B)^{-1/\xi}$. The fits provide a statistically acceptable description for all centrality classes. The values of the ξ exponent are not compatible with $\xi = 2$ (which would correspond to the hydro calculations). These interesting observations provide ample motivation for new theoretical and phenomenological studies involving hydrodynamical calculations with Lévy-type sources.

Last but not least, the correlation strength parameter λ is shown in Figure 5. It exhibits very similar behavior with m_T as the PHENIX result of ref. [17]. There is an increase and a saturation towards high m_T. The magnitude of the parameter also depends on centrality; the highest values are observed in the most central case. Reasons behind the observed m_T dependence could include in-medium mass modification of the η' meson [17] or partial coherence [4]. Within the core-halo model [32], the λ parameter is interpreted as the squared fraction of primordial pions (and decays of short-lived resonances) to all produced pions (including decays of long-lived resonances). This is, however, not yet well understood for power law sources and needs to be explored in more detail from the phenomenology side. It is also important to note that a different trend was observed at SPS energies. The NA61/SHINE experiment found no decrease at low m_T [19,43]. Hence, a beam-energy-dependent analysis could provide interesting new insights into the interpretation of this parameter as well.

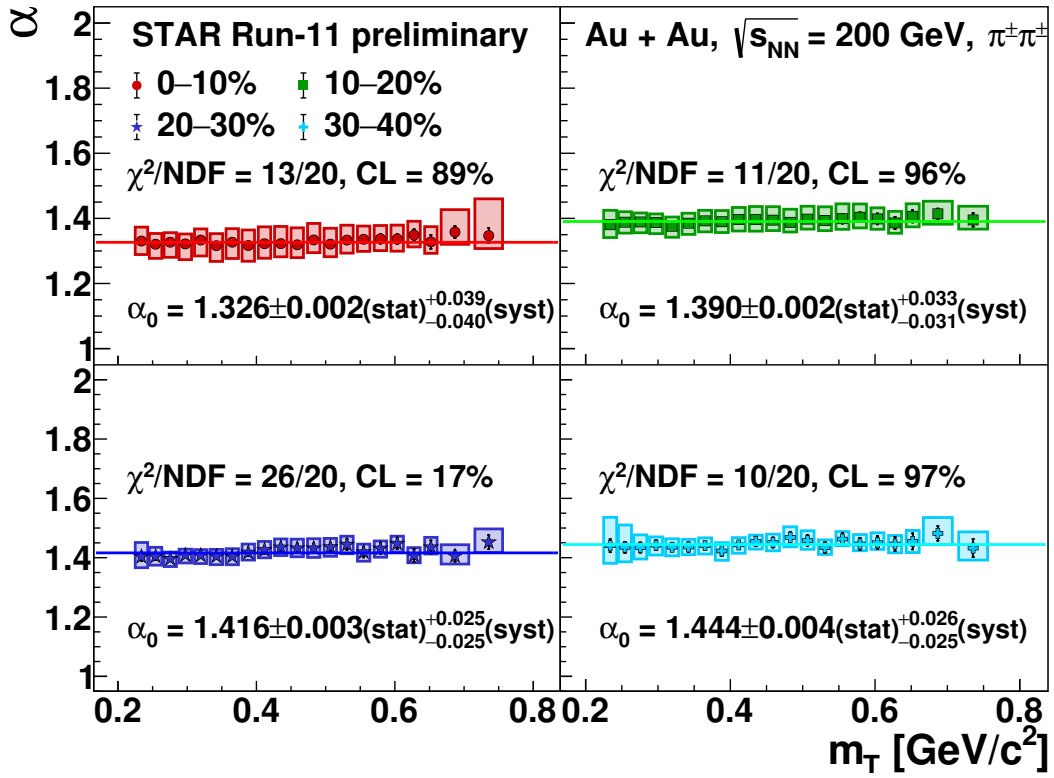

Figure 2. Average transverse momentum dependence of the Lévy exponent α parameter in Au + Au collisions at $\sqrt{s_{NN}}$ =200 GeV for four different centrality classes (0–10%, 10–20%, 20–30%, 30–40%). The m_T dependence is fitted with a constant $\alpha(m_T) = \alpha_0$ parametrization, which provides a statistically acceptable description at all four centrality classes. The colored markers and error bars correspond to the parameter values and their statistical uncertainties extracted from fits similar to Figure 1. The colored boxes correspond to the total systematic uncertainties.

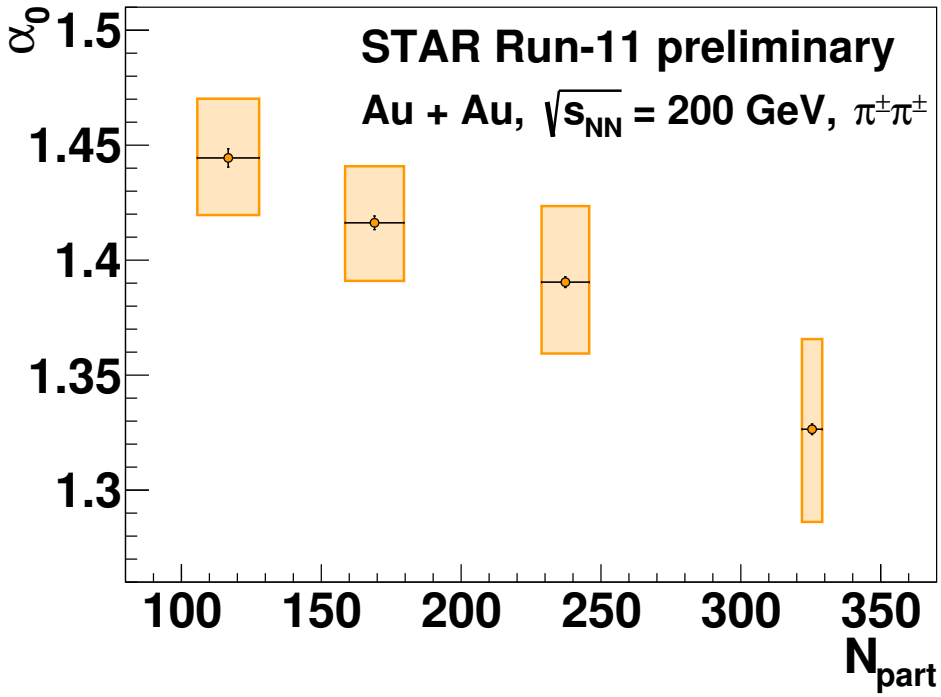

Figure 3. Number of participant nucleons dependent of the m_T-averaged Lévy exponent. The colored markers and error bars correspond to the parameter values and their statistical uncertainties extracted from the $\alpha(m_T) = \alpha_0$ constant fits. The colored boxes correspond to the total systematic uncertainties.

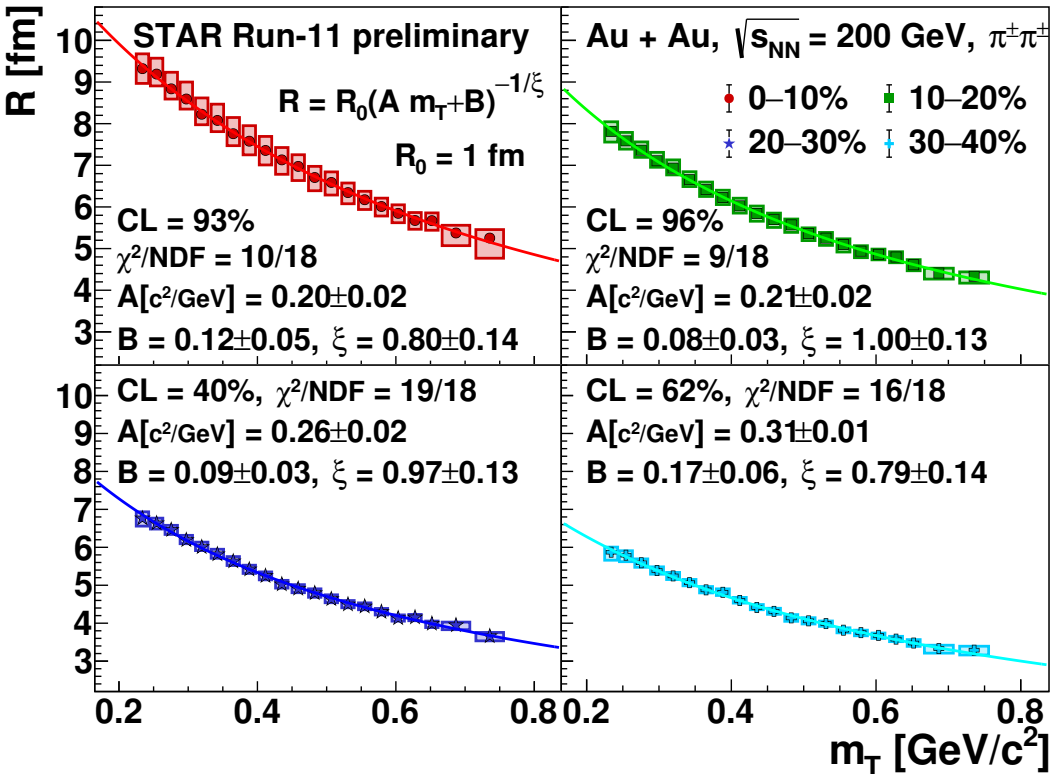

Figure 4. Average transverse momentum dependence of the Lévy scale R parameter in Au + Au collisions at $\sqrt{s_{NN}}$ =200 GeV for four different centrality classes (0–10%, 10–20%, 20–30%, 30–40%), plotted on separate panels. The m_T dependence is fitted with an $R(m_T) = R_0(Am_T + B)^{-1/\xi}$ parametrization, which provides a statistically acceptable description at all four centrality classes. The colored markers and error bars correspond to the parameter values and their statistical uncertainties extracted from fits similar to Figure 1. The colored boxes correspond to the total systematic uncertainties.

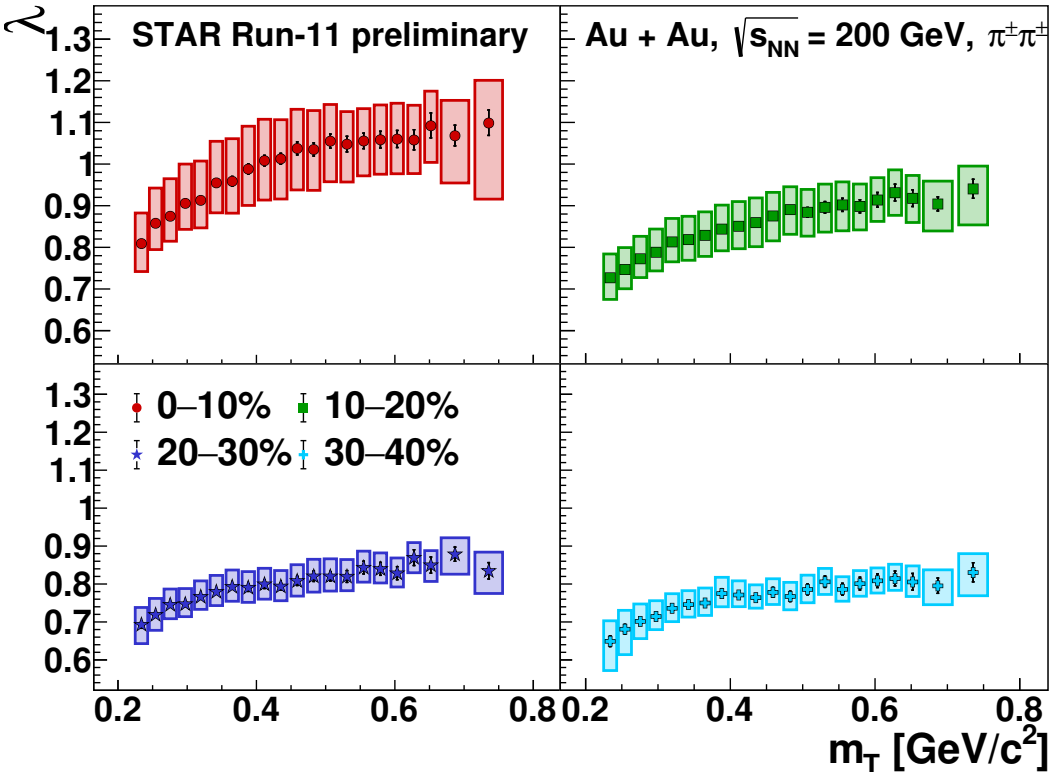

Figure 5. Average transverse momentum dependence of the correlation strength λ parameter in Au + Au collisions at $\sqrt{s_{NN}}$ =200 GeV for four different centrality classes (0–10%, 10–20%, 20–30%, 30–40%). The colored markers and error bars correspond to the parameter values and their statistical uncertainties extracted from fits similar to Figure 1. The colored boxes correspond to the total systematic uncertainties.

5. Discussion, Conclusions, and Outlook

In this paper, we presented comprehensive new preliminary results on the average transverse mass and centrality dependence of the Lévy source parameters of pion pairs. The source parameters α, R, and λ were extracted from one-dimensional momentum correlation functions measured by the STAR experiment in $\sqrt{s_{NN}}$ = 200 GeV Au + Au collisions.

The values of the Lévy exponent α were in the range of 1.3–1.5, far from the Gaussian ($\alpha = 2$) case. No m_T dependence and a decreasing trend from peripheral to central collisions were observed. The Lévy scale R parameter showed a clear centrality ordering, possibly connected to initial geometry, with the largest values observed at the most central case. A decreasing trend with m_T was also observed, similar to observations for the Gaussian HBT radii. The m_T dependence was fitted with an $R(m_T) = R_0(Am_T + B)^{-1/\xi}$ parametrization, which provided a good description at all four centrality classes. The correlation strength parameter showed an increasing trend and a saturation at high-m_T values, and a decreasing trend from central to peripheral collisions. The trends and magnitudes of the parameters are also in agreement (within systematic uncertainties) with published PHENIX results for 0–30% Au + Au collisions at the same collision energy [17].

To finalize these results, a more detailed systematic uncertainty investigation is currently underway. Furthermore, this Lévy analysis is being extended to lower collision energies recorded during the second phase of the RHIC Beam Energy Scan. Ongoing and planned investigations also include a three-dimensional analysis of the pion correlation functions and a kaon analysis. These new experimental results, together with phenomenological investigations, will hopefully shed light on the physical processes playing a role in shaping the two-particle source function in heavy-ion collisions.

Funding: This research was funded in part by the NKFIH grants K-138136, TKP2021-NKTA-64, and PD-146589.

Data Availability Statement: Data are contained within the article.

Conflicts of Interest: The authors declare no conflicts of interest.

References

1. Boal, D.H.; Gelbke, C.K.; Jennings, B.K. Intensity interferometry in subatomic physics. *Rev. Mod. Phys.* **1990**, *62*, 553–602. [CrossRef]
2. Weiner, R.M. Boson interferometry in high-energy physics. *Phys. Rep.* **2000**, *327*, 249–346. [CrossRef]
3. Wiedemann, U.A.; Heinz, U.W. Particle interferometry for relativistic heavy ion collisions. *Phys. Rep.* **1999**, *319*, 145–230. [CrossRef]
4. Csörgő, T. Particle interferometry from 40-MeV to 40-TeV. *Acta Phys. Hung. A* **2002**, *15*, 1–80. [CrossRef]
5. Kisiel, A. Overview of the femtoscopy studies in Pb Pb and pp collisions at the LHC by the ALICE experiment. In Proceedings of the Seventh Workshop on Particle Correlations and Femtoscopy, Tokyo, Japan, 20–24 September 2011; p. 3. [CrossRef]
6. Lisa, M.A.; Pratt, S.; Soltz, R.; Wiedemann, U. Femtoscopy in relativistic heavy ion collisions. *Ann. Rev. Nucl. Part. Sci.* **2005**, *55*, 357–402. [CrossRef]
7. Lednicky, R. Femtoscopy with unlike particles. In Proceedings of the International Workshop on the Physics of the Quark Gluon Plasma, Palaiseau, France, 4–7 September 2001.
8. Acharya, S. et al. [ALICE Collaboration] Pion-kaon femtoscopy and the lifetime of the hadronic phase in Pb-Pb collisions at $\sqrt{s_{\rm NN}}$ = 2.76 TeV. *Phys. Lett. B* **2021**, *813*, 136030. [CrossRef]
9. Landau, L.D.; Lifshits, E.M. Quantum Mechanics: Non-Relativistic Theory. In *Course of Theoretical Physics*; Butterworth-Heinemann: Oxford, UK, 1991; Volume v.3.
10. Pratt, S. Validity of the smoothness assumption for calculating two-boson correlations in high-energy collisions. *Phys. Rev. C* **1997**, *56*, 1095–1098. [CrossRef]
11. Brown, D.A.; Danielewicz, P. Imaging of sources in heavy-ion reactions. *Phys. Lett. B* **1997**, *398*, 252–258. [CrossRef]
12. Adler, S.S. et al. [PHENIX Collaboration] Evidence for a long-range component in the pion emission source in Au + Au collisions at s(NN)**(1/2) = 200-GeV. *Phys. Rev. Lett.* **2007**, *98*, 132301. [CrossRef]
13. Kincses, D.; Stefaniak, M.; Csanád, M. Event-by-Event Investigation of the Two-Particle Source Function in Heavy-Ion Collisions with EPOS. *Entropy* **2022**, *24*, 308. [CrossRef]
14. Kórodi, B.; Kincses, D.; Csanád, M. Event-by-event investigation of the two-particle source function in sNN = 2.76 TeV PbPb collisions with EPOS. *Phys. Lett. B* **2023**, *847*, 138295. [CrossRef]
15. Nagy, M.; Purzsa, A.; Csanád, M.; Kincses, D. A novel method for calculating Bose–Einstein correlation functions with Coulomb final-state interaction. *Eur. Phys. J. C* **2023**, *83*, 1015. [CrossRef]
16. Kurgyis, B.; Kincses, D.; Nagy, M.; Csanád, M. Coulomb Corrections for Bose–Einstein Correlations from One- and Three-Dimensional Lévy-Type Source Functions. *Universe* **2023**, *9*, 328. [CrossRef]
17. Adare, A. et al. [PHENIX Collaboration] Lévy-stable two-pion Bose-Einstein correlations in $\sqrt{s_{NN}} = 200$ GeV Au + Au collisions. *Phys. Rev. C* **2018**, *97*, 064911; Erratum in *Phys. Rev. C* **2023**, *108*, 049905. [CrossRef]
18. Tumasyan, A.; CMS Collaboration. Two-Particle Bose-Einstein Correlations and Their Lévy Parameters in PbPb Collisions at $\sqrt{s_{\rm NN}}$ = 5.02 TeV. 2023. Available online: https://arxiv.org/abs/2306.11574 (accessed on 19 February 2024).
19. Adhikary, H.; NA61/SHINE Collaboration. Two-pion femtoscopic correlations in Be + Be collisions at $\sqrt{s_{\rm NN}} = 16.84$ GeV measured by the NA61/SHINE at CERN. *Eur. Phys. J. C* **2023**, *83*, 919. [CrossRef]
20. Nolan, J.P. *Univariate Stable Distributions*; Springer Series in Operations Research and Financial Engineering; Springer: New York, NY, USA, 2020. [CrossRef]
21. Csörgő, T.; Hegyi, S.; Zajc, W.A. Bose-Einstein correlations for Levy stable source distributions. *Eur. Phys. J. C* **2004**, *36*, 67–78. [CrossRef]
22. Gnedenko, B.V.; Kolmogorov, A.N.; Chung, K.L. *Limit Distributions for Sums of Independent Random Variables*; Addisson-Wesley: Cambridge, MA, USA, 1954.
23. Csörgő, T.; Hegyi, S.; Novák, T.; Zajc, W.A. Bose-Einstein or HBT correlations and the anomalous dimension of QCD. *Acta Phys. Polon. B* **2005**, *36*, 329–337.
24. Achard, P.; L3 Collaboration. Test of the τ-Model of Bose-Einstein Correlations and Reconstruction of the Source Function in Hadronic Z-boson Decay at LEP. *Eur. Phys. J. C* **2011**, *71*, 1648. [CrossRef]
25. Csörgő, T.; Hegyi, S.; Novák, T.; Zajc, W.A. Bose-Einstein or HBT correlation signature of a second order QCD phase transition. *AIP Conf. Proc.* **2006**, *828*, 525–532. [CrossRef]
26. Tomášik, B.; Cimerman, J.; Plumberg, C. Averaging and the Shape of the Correlation Function. *Universe* **2019**, *5*, 148. [CrossRef]
27. Cimerman, J.; Tomášik, B.; Plumberg, C. The Shape of the Correlation Function. *Phys. Part. Nucl.* **2020**, *51*, 3. [CrossRef]
28. Csanád, M.; Csörgő, T.; Nagy, M. Anomalous diffusion of pions at RHIC. *Braz. J. Phys.* **2007**, *37*, 1002–1013. [CrossRef]
29. Metzler, R.; Barkai, E.; Klafter, J. Anomalous Diffusion and Relaxation Close to Thermal Equilibrium: A Fractional Fokker-Planck Equation Approach. *Phys. Rev. Lett.* **1999**, *82*, 3563–3567. [CrossRef]

30. Csanád, M.; Kincses, D. Femtoscopy with Lévy sources from SPS through RHIC to LHC. *Universe* **2024**, *10*, 54. [CrossRef]
31. Kurgyis, B. Three dimensional Lévy HBT results from PHENIX. In Proceedings of the 13th Workshop on Particle Correlations and Femtoscopy 2018, Krakow, Poland , 26–29 May 2018. [CrossRef]
32. Csörgő, T.; Lörstad, B.; Zimányi, J. Bose-Einstein correlations for systems with large halo. *Z. Phys. C* **1996**, *71*, 491–497. [CrossRef]
33. Csanád, M.; Jakovác, A.; Lökös, S.; Mukherjee, A.; Kumar, T.S. Multi-particle quantum-statistical correlation functions in a Hubble-expanding hadron gas. In *Gribov-90 Memorial Volume*; World Scientific: Singapore, 2020; pp. 261–273. [CrossRef]
34. Anderson, M.; Berkovitz, J.; Betts, W.; Bossingham, R.; Bieser, F.; Brown, R. The Star time projection chamber: A Unique tool for studying high multiplicity events at RHIC. *Nucl. Instrum. Meth. A* **2003**, *499*, 659–678. [CrossRef]
35. Shao, M.; Barannikova, O.Y.; Dong, X.; Fisyak, Y.; Ruan, L.; Sorensen, P.; Xu, Z. Extensive particle identification with TPC and TOF at the STAR experiment. *Nucl. Instrum. Meth. A* **2006**, *558*, 419–429. [CrossRef]
36. Wu, J.; Xu, M. A barrel TOF for STAR at RHIC. *J. Phys. G* **2007**, *34*, S729–S732. [CrossRef]
37. Llope, W.J. Large-Area Fast-Timing Systems In STAR. *AIP Conf. Proc.* **2011**, *1336*, 569. [CrossRef]
38. Adams, J. et al. [STAR Collaboration] Pion interferometry in Au + Au collisions at $\sqrt{s_{NN}}$ = 200 GeV. *Phys. Rev. C* **2005**, *71*, 044906. [CrossRef]
39. Adamczyk, L. et al. [STAR Collaboration] Beam-energy-dependent two-pion interferometry and the freeze-out eccentricity of pions measured in heavy ion collisions at the STAR detector. *Phys. Rev. C* **2015**, *92*, 014904. [CrossRef]
40. Makhlin, A.N.; Sinyukov, Y.M. Hydrodynamics of Hadron Matter Under Pion Interferometric Microscope. *Z. Phys. C* **1988**, *39*, 69. [CrossRef]
41. Csörgő, T. and Lörstad, B. Bose-Einstein correlations for three-dimensionally expanding, cylindrically symmetric, finite systems. *Phys. Rev. C* **1996**, *54*, 1390–1403. [CrossRef] [PubMed]
42. Lisa, M.A.; Pratt, S. Femtoscopically Probing the Freeze-out Configuration in Heavy Ion Collisions. In *Landolt-Börnstein—Group I Elementary Particles, Nuclei and Atoms*; Springer: Berlin/Heidelberg, Germany, 2010; Chapter 21. [CrossRef]
43. Pórfy, B. Femtoscopic Correlation Measurement with Symmetric Lévy-Type Source at NA61/SHINE. *Universe* **2023**, *9*, 298. [CrossRef]